Turkish Journal of Physics

Volume 22 | Number 2 Article 8

1-1-1998

An Analysis of the Variation in Calculated Confined-State Energies Using Different Envelope-Function Models

Beşire GÖNÜL

Follow this and additional works at: https://journals.tubitak.gov.tr/physics

 Part of the Physics Commons

Recommended Citation

GÖNÜL, Beşire (1998) "An Analysis of the Variation in Calculated Confined-State Energies Using Different Envelope-Function Models," *Turkish Journal of Physics*: Vol. 22: No. 2, Article 8. Available at: https://journals.tubitak.gov.tr/physics/vol22/iss2/8

This Article is brought to you for free and open access by TÜBİTAK Academic Journals. It has been accepted for inclusion in Turkish Journal of Physics by an authorized editor of TÜBİTAK Academic Journals. For more information, please contact academic.publications@tubitak.gov.tr.

Tr. J. of Physics
22 (1998) , 157 – 167.
© TÜBİTAK

An Analysis of the Variation in Calculated Confined-State Energies Using Different Envelope-Function Models

Beşire GÖNÜL
Department of Engineering Physics
University of Gaziantep, 27310 Gaziantep - TURKEY

Received 20.02.1997

Abstract

We investigate different formulations of the envelope-function method and show that the accuracy of the calculated zone-centre confinement energies can be calculated by means of bulk band structure. We show how coupling to the conduction and spin-split-off bands can decrease the light-hole zone-centre confinement energies and lead to significant differences in the calculated subband dispersion.

1. Introduction

One of the major themes to emerge in the study of quantum well lasers is the key role of the valence band states in determining the lasing properties of any quantum well (QW) structure. An accurate description of the gain as a function of carrier or current density therefore requires a careful analysis of the valence band states in the quantum well structure. The envelope function method is commonly used to investigate the band structure of layered semiconductor structures. The numerical solution of the multicomponent envelope-function Hamiltonian is difficult; therefore a variety of different simplifications have been used in the literature.

In this paper, the valence band structure is calculated using Hamiltonians based on different numbers of bulk bands. It is seen that when we consider explicitly the off-diagonal mixing of the conduction-and valence-bands or include the spin-split-off band, the light-hole band nonparabolicity is increased and the energies of the light-hole subbands are decreased. It is shown that the accuracy of the calculated zone-centre subband energies and dispersions can be simply predicted by plotting the equivalent bulk band structure for an infinitely deep quantum well using the different starting Hamiltonians.

Some analytical expressions are also presented to calculate valence subband zone-centre confinement energies.

In Section 2 we present the envelope-function Hamiltonian and the different band models based on the Hamiltonian. We present the analytical expressions for the calculation of zone-centre confinement energies for valence bands in Section 3. We demonstrate in Section 4 that the effects of nonparabolicity on zone-centre confined-state energies can be predicted directly from the bulk band structure for an infinitely deep QW structure. In Section 5 we use the envelope function Hamiltonian to calculate the subband dispersion in the quantum well plane for different band models, make comments concerning the effects of nonparabolicity and well width on subband dispersion in an infinite quantum well structure and consider also the influence of the spin-split-off band. We show how the inclusion of the conduction and spin-split off bands affects the position of the light holes at $k_{||} = 0$.

2. Envelope-Function Hamiltonians

In this section we describe the different envelope function Hamiltonians used in the calculations. The eight-band **k.p** Hamiltonian is based on the six highest valence bands and two lowest conduction bands at the Γ point, typically including all interactions between these bands up to order k^2. One of the most important advantages of the eight-band model is that it treats equally all of the bands explicitly included in the calculation. In order to simplify the numerical solution of the eight-band model, it is common to block diagonalize it into two 4×4 Hamiltonians [1], which can be further simplified by introducing the axial approximation [2], which retains the exact dispersion along the z-direction (when $k_x = k_y = 0$) but modifies the Hamiltonian so that it is axially symmetric in the $x - y$ plane. Thus, the block diagonalized extended **k.p** Hamiltonian for an unstrained semiconductor is given in the axial approximation by [1],

$$H = \begin{bmatrix} E_{CB} & P_1 & P_2 & P_3 \\ P_1^* & E_{HH} & A & B \\ P_2^* & A^* & E_{LH} & C \\ P_3^* & B^* & C^* & E_{SO} \end{bmatrix}, \tag{1}$$

where the diagonal matrix elements of H are defined as

$$\begin{aligned} E_{CB} &= E_g + E_{co} + \left(F + \frac{1}{2}\right) k_t^2 + \left(F + \frac{1}{2}\right) k_z^2, \\ E_{HH} &= E_{\nu o} - \frac{1}{2}(\gamma_1 - 2\gamma_2) k_z^2 - \frac{1}{2}(\gamma_1 + \gamma_2) k_t^2, \end{aligned} \tag{2}$$

$$E_{LH} = E_{\nu o} - \frac{1}{2}(\gamma_1 + 2\gamma_2) k_z^2 - \frac{1}{2}(\gamma_1 - \gamma_2) k_t^2,$$

$$E_{SO} = E_{\nu o} - \Delta - \frac{1}{2}\gamma_1 k_z^2 - \frac{1}{2}\gamma_1 k_t^2. \tag{3}$$

Here, γ_1, γ_2 and γ_3 are related to the true Luttinger parameters, which will be described below; Δ is the magnitude of the spin-orbit energy at $k = 0$; and E_{co} and $E_{\nu o}$ are the Γ-point conduction and valence-band-edge energies. The off-diagonal matrix elements of H are given by

$$\begin{aligned} P_1 &= -(1/\sqrt{2})Pk_z, \\ P_2 &= (\sqrt{2}/\sqrt{3})Pk_z + i/\sqrt{6})Pk_{||}, \\ P_3 &= -(1/\sqrt{3})Pk_z + (i/\sqrt{3})Pk_{||}, \\ A &= \sqrt{3}\gamma_3 k_{||}k_z + i(\sqrt{3}/2)\gamma k_{||}^2, \\ B &= -(\sqrt{3}/\sqrt{2})\gamma_3 k_{||}k_z + i(\sqrt{3}/\sqrt{2})\gamma k_{||}^2, \\ C &= \sqrt{2}\gamma_2 k_z^2 - (1/\sqrt{2})\gamma_2 k_{||}^2 - i(3/\sqrt{2})\gamma_3 k_{||}k_z, \\ k_{||}^2 &= k_x^2 + k_y^2, \quad \gamma = \frac{1}{2}(\gamma_2 + \gamma_3), \end{aligned} \tag{4}$$

where P is the Kane matrix element [3]. We have taken $\hbar = m = 1$. The axial approximation involves introducing the term γ in A and B. The parameters γ_i are related to the true valence-band Luttinger parameters γ_i^L by the relations [4]

$$\begin{aligned} \gamma_1^L &= \gamma_1 + E_p/(3E_g), \\ \gamma_2^L &= \gamma_2 + E_p/(6E_g), \\ \gamma_3^L &= \gamma_3 + E_p/(6E_g), \end{aligned} \tag{5}$$

where E_g is the fundamental band gap and E_p is related to the Kane matrix element P by $E_p = 2mP^2/\hbar^2$. The coupling between the conduction and valence bands is explicity included in the eight-band model. In the **k.p** approach there are seven bulk band structure parameters $E_g, P, F, \Delta, \gamma_1, \gamma_2$ and γ_3. Since the fundamental band gap E_g and the spin-orbit energy Δ can be determined independently as a function of composition and temperature, we therefore take them as fixed when calculating the other five parameters from the measured or estimated effective masses namely, $m_c^*, m_{hh}^*, m_{lh}^*$ and m_{so}^* in the (001) direction and m_{hh}^* in the (111) direction. The eigenvalues of the blocked Hamiltonian for the bulk case, calculated up to second order in the components of the momentum $\mathbf{k}$, can be used to determine the effective mass for each band in the vicinity of the Γ point. The Γ_6 effective mass m_c^* is given [1] by,

$$m_c^{*-1} = 1 + 2F + \frac{E_p}{3}\left[\frac{2}{E_g} + \frac{1}{E_g + \Delta}\right], \tag{6}$$

which shows the band gap and spin-orbit energy dependence of the conduction band effective mass. Also, the heavy-hole effective mass along the (001) direction is determined only by the parameters γ_1, γ_2 as

$$m_{hh}^\star = (\gamma_1 - 2\gamma_2)$$

whereas in the same direction the light hole effective mass is coupled to the conduction band as

$$m_{lh}^{*-1} = (\gamma_1 + 2\gamma_2) + \left[\frac{2E_p}{3E_g}\right]. \tag{7}$$

On the other hand, the heavy-hole effective mass in the (111) direction depends only on γ_1 and γ_3 and is given by

$$m_{hh}^{*-1} = (\gamma_1 - 2\gamma_3). \tag{8}$$

Finally, the effective mass of the split-off branch is given by

$$m_{so}^{*-1} = \gamma_1 + \frac{E_p}{3E_g}\left(\frac{E_g}{E_g + \Delta}\right). \tag{9}$$

It can be noticed from Eqs. (5)-(9) that in the eight-band **k.p** model the light-hole and split-off bands are both coupled to the lowest conduction band, whereas the heavy-hole effective mass is not.

Four different models based on the Hamiltonian of Eq. (1) is considered. These are (i) the four-band model, with coupled CB, HH, LH, and SO bands (solid line); (ii) a three-valence band model, with coupled HH, LH, and SO bands, and a parabolic CB (dotted line); (iii) a two-band model, with coupled HH and LH, a parabolic conduction band, and the split-off band neglected (dashed line); and (iv) a mixed three-band model, with coupled CB, HH, and LH, and neglecting the SO band (dotted-dashed line). CB stands for conduction band, HH stands for heavy-hole band, LH stands for light-hole band, and SO for spin-split-off band. In models (ii) and (iii), we use the true Luttinger parameters γ_i^L, whereas in (i) and (iv) we use the valence-band effective mass parameters γ_i. These two sets of parameters are related by Eq. (4). In model (i) the term 1+F replaces the inverse bulk band edge conduction band mass since we have now explicitly included the coupling to the top valence bands. This is obtained from the experimental conduction band mass Eq. (5). To obtain the matrix eigenvalue equation for the quantum well subband dispersion, we replace k_z by the operator $-i\partial/\partial z$ for quantum wells grown along the (001) direction.

3. Infinite Well Hamiltonian

In this section, we apply the envelope-function Hamiltonian of Eq. (1) to demonstrate that the zone-centre confined-state energies in an infinitely deep quantum well can be determined directly from a plot of the bulk band dispersion along the growth direction. At the centre of the two-dimensional Brillouin zone, where $k_{||} = 0$, Eq. (1) decouples into two independent matrices, a 1×1 matrix describing the heavy-hole dispersion and a 3×3 matrix,

$$H = \begin{vmatrix} E_g + \left(F + \frac{1}{2}\right) k_z^2 & (\sqrt{2}/\sqrt{3})Pk_z & -(1/\sqrt{3})Pk_z \\ (\sqrt{2}/\sqrt{3})Pk_z & -\frac{1}{2}(\gamma_1 + 2\gamma_2)k_z^2 & \sqrt{2}\gamma_2 k_z^2 \\ -(1/\sqrt{3})Pk_z & \sqrt{2}\gamma_2 k_z^2 & -\Delta - \frac{1}{2}\gamma_1 k_z^2 \end{vmatrix} \tag{10}$$

which needs to be solved to calculate the (mixed) CB, LH, and SO confined-state energies. Because of this decoupling, the heavy-hole zone-centre confined-state energies are identical in the four models considered above. If we take $E_{\nu o} = 0$, the heavy-hole bulk dispersion along k_z is given by

$$E_{HH}(k_z) = -\frac{1}{2}(\gamma_1 - 2\gamma_2)k_z^2. \tag{11}$$

If we define the quantum well between $z = 0$ and L, and apply the boundary conditions that the envelope function $f(z)$ goes to zero at the interfaces [5], we find that the heavy-hole confined states are standing waves with wave vector $k_z = n\pi/L$. The envelope functions are given by

$$f(z) = \begin{cases} \sqrt{2/L}\sin(n\pi z/L) & 0 < z < L \\ 0 & \text{otherwise} \end{cases} \tag{12}$$

and the confined-state energies for heavy-holes are found directly from the bulk band structure by replacing k_z by $n\pi/L$ in Eq. (11).

The remaining 3×3 matrix of Eq. (10) can be solved using an expansion in diagonal (uncoupled) states [6, 7]. We consider the calculation of a confined-state predominantly of light-hole character, for which the light-hole component of the envelope function varies as $f_{LHm}(z) = \sin(m\pi z/L)$. If we allow the split-off component of the wave function also to vary as $f_{sop}(z) = \sin(p\pi z/L)$, then the off-diagonal term involving k_z^2 introduces a direct mixing between the normalized light-hole and split-off components such that [7]

$$\langle f_{sop}(z)| - \partial^2/\partial z^2 | f_{LHm}(z)\rangle = (m\pi/L)^2\delta_{pm}, \tag{13}$$

i.e., the only direct mixing between f_{LHm} and the split-off band is with f_{som} and the magnitude of the interaction is found by replacing k_z^2 by $(m\pi/L)^2$ in the 3×3 matrix. Finally, the terms P_2 and P_3 linking the conduction band to the light-hole band and split-off bands are both of order k_z. Taking the conduction-band envelope function as $f_{CBq}(z) = icos(q\pi z/L)$ [8], we conclude that f_{LHm} and f_{SOm} mix only with the conduction-band component f_{CBm}, with the magnitude of the interaction found by replacing k_z in $P_{2,3}$ by $m\pi/L$ in Eq. (1). Hence, the zone-centre energy of the mth LH, SO, and CB confined states in an infinite quantum well can be found by replacing each occurrence of k_z in Eq. (1) with $m\pi/L$.

The zone-centre confined-state energies in an infinite well of width L are then just equal to the bulk band energies at $k_z = m\pi/L$ for each of the four calculation models described above. We thus conclude that in an infinite well the difference between the calculated confined-state energies using different models can be predicted directly from the differences in the bulk structures.

We further note that, the zone centre LH and SO confined state energies can be determined analytically in the HH+LH+SO model by finding the eigenvalues of

$$\det[H_{ij} - \delta_{ij}E] = 0 \tag{14}$$

where H_{ij} is the 2×2 Hamiltonian for the LH and SO bands at $k_{||} = 0$:

$$H = \begin{bmatrix} D_+ & C_- \\ C_- & D_- \end{bmatrix}. \tag{15}$$

The matrix elements in (15) are given by

$$D_+ = -\frac{1}{2}(\gamma_1 + 2\gamma_2)k_z^2, \tag{16}$$

$$D_- = -\Delta - \frac{1}{2}\gamma_1 k_z^2, \tag{17}$$

and

$$C_- = \sqrt{2}\gamma_2 k_z^2. \tag{18}$$

Solution of Eq. (14) gives the zone centre confinement energies for the LH and SO subbands as

$$E_{LH,SO} = \frac{(D_+ + D_-) \pm \sqrt{(D_+ + D_-)^2 - 4(D_+D_- - C_-^2)}}{2}, \tag{19}$$

where the + and - signs correspond to the LH- and SO-subbands, respectively. The energy of the nth LH and SO confined states can then be found by replacing k_z by $n\pi/L$ in Eqs. (16)-(18).

4. Valence-Subband Dispersion and Zone-Centre Confined-State Energies

In this section we show that the accuracy of the calculated zone-centre energies in an infinite QW using different models can be predicted by plotting the equivalent bulk band structures $E(k_z, k_{||})$ by taking $k_{||} = 0$ and k_z as a number. We first calculate the variation of confined-state energy with well width for $GaAs$ infinite quantum wells with a spin-orbit energy of 343 meV. To illustrate the effect of the spin-split-off band we then repeat the calculations assuming a spin-orbit energy of 800 meV.

Since we are primarily interested in investigating trends in the different band models as a function of spin-split-off energy, we use the spherical approximation, obtained by replacing γ_2^L and γ_3^L by a suitable average value:

$$\gamma_2 = \gamma_3 = \frac{(3\gamma_3 + 2\gamma_2)}{5}. \tag{20}$$

The band-structure parameters used here and in later sections are listed in Table 1.

Figure 1 (a) illustrates the light-hole dispersion of bulk GaAs calculated using models (i) CB, LH, and SO mixing at the zone centre (dashed line), (ii) coupled LH and SO bands (solid line), and (iii) the LH band model (dotted line). The bulk light-hole band dispersion calculated using models (i) and (ii) are very close to each other, up to about 60 meV below the band edge, and we find that the calculated confined-state energies for GaAs infinite quantum wells (see Figure 1 (b)), are also in close agreement in this energy range. It is seen from Figure 1(a) that interactions with both the conduction band and split-off band increase the light-hole band nonparabolicity.

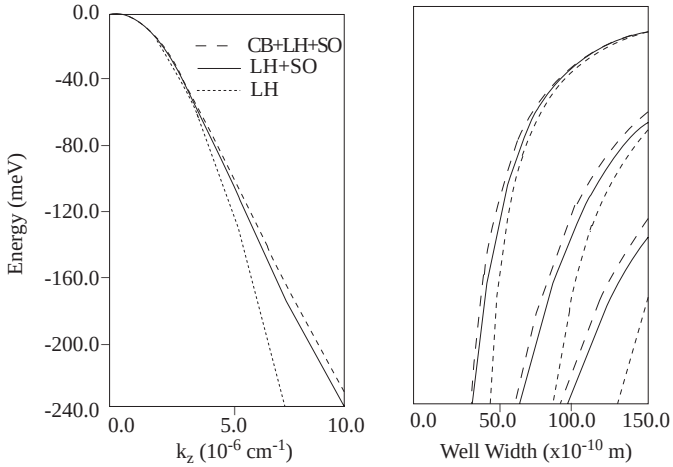

Figure 1. (a) Dispersion of the light-hole band in bulk GaAs with a spin-orbit energy of 343 meV calculated using the three different Hamiltonians, described in the text.
(b) Energy of the light-hole states as a function of well width in an infinite GaAs quantum well, using the three Hamiltonians.

It is seen from Figure 1 that for a fixed well width L, the differences in the n^{th} calculated zone-centre confinement energies in an infinite quantum well are equal to those calculated for the bulk band dispersion along the growth direction at a fixed wavevector $k_z = n\pi/L$, as predicted. This result is modified in a finite quantum well, where the difference between the calculated confinement energies using different band models increases with confined-state index, approaching the difference in bulk band energies for the highest confined states, as we have shown recently [8].

We repeat the calculations of Figure 1 assuming the spin-orbit-energy is 800 meV to see how the split-off band affects the bulk subband dispersion and confinement energies of light-hole states.

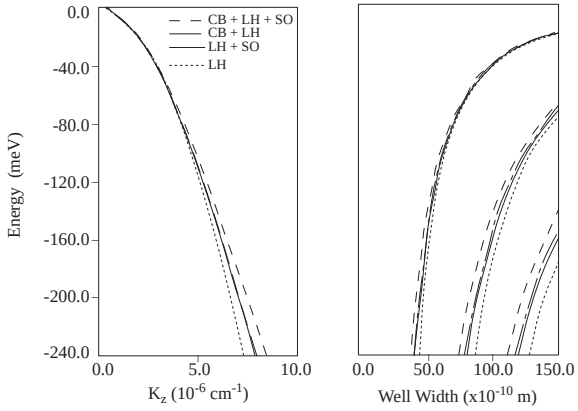

Figure 2. (a) Dispersion of the light-hole band in bulk GaAs assuming a spin-orbit energy of 800 meV using four different Hamiltonians. (b) Energy of the light-hole states as a function of well width in an infinite GaAs quantum well, using the three Hamiltonians

This is shown in Figure 2 where we have now also included model (iv), with coupled CB and LH (dot dashed line). Due to the wide band-gap and large spin-orbit energy, a similar band dispersion is found in models (ii) LH + SO and (iv) CB + LH implying the equal importance of the CB and SO in this energy range. We would thus predict that the calculated confinement energies should also be similar in the two models, and this is indeed found to be the case. The comparison of Figs. 1 and 2 show clearly that as the spin-orbit-splitting increases from 343 meV to 800 meV, the nonparabolicity is also reduced and hence the differences decrease between the calculated zone-centre confinement energies using the different models.

Overall, we conclude from Figs. 1 and 2 that the accuracy of the calculated zone-centre energies under different approximations can be well estimated by using different models to plot the bulk band structure along the growth direction.

5. Valence-Subband Structure of Infinite Quantum Wells

In this section we consider the valence-subband dispersion, which is complicated due to the interactions between the different subbands that lead to band mixing effects [7]. It is instructive to compare the infinite quantum well valence band dispersion in different models.

In Figure 3 we present the calculated valence subband dispersion for 100 Å GaAs infinite quantum well as a function of in-plane wavevector k_x.

We use the full fourband Hamiltonian of Eq. 1 with coupled CB, HH, LH, and SO (dashed line), a three valence band model with coupled HH, LH, and SO (solid line), and a two band model with coupled HH and LH (dotted line).

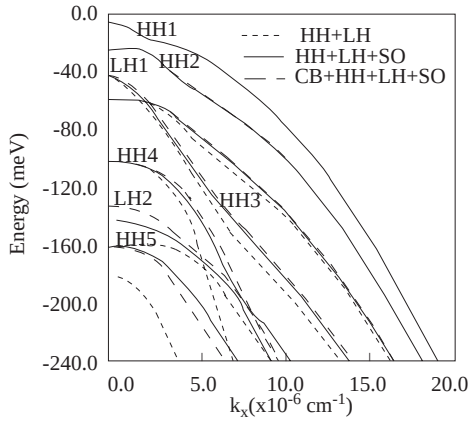

Figure 3. Valence-subband dispersion of a 100 Å GaAs infinite quantum well, calculated with the following bands included explicitly in the calculation (dotted line) HH and LH only, (solid line) HH, LH, and SO, (dashed line) CB, HH, LH and SO.

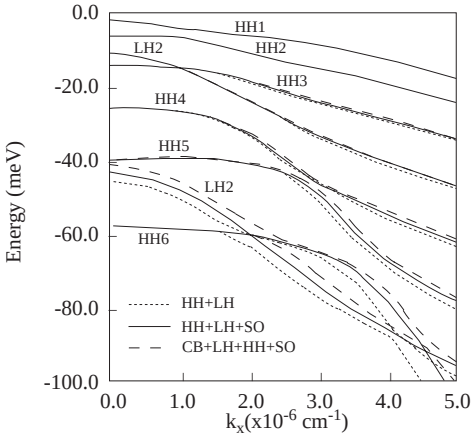

Figure 4. Valence-subband dispersion of a 200 Å GaAs infinite quantum well, calculated with the following bands included explicitly in the calculation (dotted line) HH and LH only, (solid line) HH, LH, and SO, (dashed line) CB, HH, LH and SO.

The valence subband mixing appears even at small values of k_x, as evidenced by the anticrossing regions. This band mixing effect is of different magnitude for each subband, depends mainly on the γ_3 term in A in Eq. 1. At large values of k_x the quadratic terms will become dominant, and, therefore the dispersions approach parabolic curvatures at large wavevector k_x.

We find in Figure (3) that the calculated band dispersion of the first heavy-hole state is practically the same throughout the whole wavevector range for the three band models considered. Differences in the subband dispersion start to appear when the calculated zone-centre confinement-energy of the light-hole subband varies with the different band models (notice the differences in the subband dispersion of HH2, LH1 and HH3 in the different models). The differences in subband dispersion become more pronounced as the calculated differences in LH zone-centre confinement-energy increase (notice the differences in subband dispersion of HH4, LH2, and HH5 with the different band models). In summary, the differences in subband dispersions increase as the calculated zone-centre energy differences increase.

The effect of decreasing the confinement energy can be seen in Figure 4, where we present the valence band dispersion for a 200 Å GaAs infinite quantum well. As the well width increases from 100 Å to 200 Å , the level separation decreases, and this leads to an enhancement of the valence band mixing and a change in the subband energy separations. The region where the effects of the diagonal and off-diagonal quadratic terms overcome

the k-linear ones also depends on the well width. It is again shown in Figure 4 that the difference between valance-subband dispersion in the two-band and many-band models increases with an increase in the calculated zone-centre light-hole confinement energy difference in the two-band and many-band models.

We have also investigated the influence of the magnitude of the spin-orbit energy on the valence subband dispersion. To demonstrate the effects of large spin-orbit energy we repeat the calculations of Figure 3 assuming a spin-orbit energy of 800 meV. We would expect, because of the large spin-orbit energy, that the calculated subband dispersion should only vary very weakly depending on whether the split-off band is included (solid and dashed line) or not (dotted and dotted dashed line) in the calculation. This is indeed found to be the case. The comparison of Figures 3 and 5 show that the models which includes CB and SO get closer to the two band model of HH+LH due to the large-spin-orbit energy.

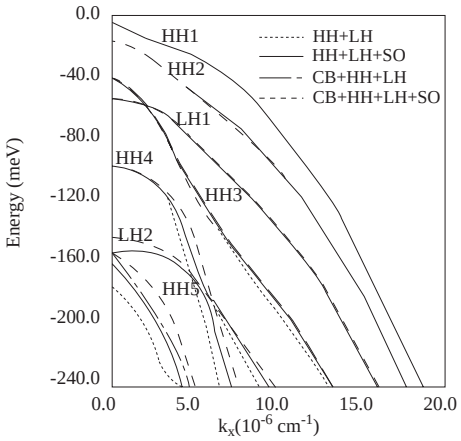

Figure 5. Valence-subband dispersion of a 100 Å GaAs infinite QW with a spin-orbit energy of 800 meV, calculated for the stated band models.

As we have shown in reference [8], the main differences found between subband dispersions in quantum wells using different band models can be predicted simply from a plot of the bulk band structure as a function of $E(n\pi/L, k_x)$, which can then serve as an adequate guide in selecting the Hamiltonian model for a specific problem.

6. Summary and Conclusions

In this paper, the envelope-function method was used to calculate confinement energies in infinite quantum wells under various approximations. We found that the differences between the various bulk band structures provide a good guide to the resulting differences in calculated confined-state energies.

We have investigated the influence of the conduction band and the spin-split-band on the valence-subband dispersion in an infinite quantum-well using a two band HH+LH model, and three other band models of **k.p** Hamiltonians, including HH+LH+SO, CB+HH+LH, and CB+HH+LH+SO, respectively. We found that the inclusion of the CB and SO coupling start to affect the subband dispersion when the calculated confinement energy of the light-holes varies significantly between the different band models.

For GaAs infinite quantum wells we found marked differences between the light-hole band structures calculated using the different **k.p** Hamiltonians. Our results demonstrated how the effect of nonparabolicity on light-hole confined-state energies becomes more marked with increasing confined-state index.

Table 1. Material parameters for GaAs.

m_c^*	0.0665
γ_1^L	6.85
γ_2^L	2.58
γ_3^L	2.58
$E_g(eV)$	1.42
$\Delta(eV)$	0.343
$E_p(eV)$	24

Acknowledgements

The author gratefully acknowledges many useful discussions with Prof.Dr. E.P. O'Reilly and financial support of the Turkish Government during the course of this work.

References

[1] A.M. Cohen, and G.E. Marques, Phys. Rev. **B41** (1990) 10 608.

[2] M. Altarelli, U. Ekenberg and A. Fasolino, Phys. Rev. **B32** (1985) 5138.

[3] E.O. Kane, in Handbook on Semiconductor edited by W. Paul (North-Holland. Amsterdam, 1982), Vol.1, p.193.

[4] C.R. Pidgeon and R.N. Brown, Phys. Rev. **146** (1966) 575.

[5] M.G. Burt, J. Phys. Condens. Matter **4** (1992) 6651.

[6] W. Batty, U. Ekenberg, A. Ghiti and E.P. O'Reilly, Semicond. Sci. Technol. **4** (1989) 904.

[7] E.P. O'Reilly, Semicond. Sci. Technol. **4** (1989) 121.

[8] A.T. Meney, Beşire Gönül and E.P. O'Reilly, Phys. Rev. **B50** (1994) 10 893.